ROLE OF TYLOSES IN THE DURABILITY OF CHESTNUT OAK

Wolfgang Ruppitsch
Former Intern
E-mail: wruppitsch.htb-b2017@fh-salzburg.ac.at

Patricia Lebow
Research Mathematical Statistician
E-mail: patricia.k.lebow@usda.gov

Stan Lebow†
Research Forest Products Technologist
Forest Service Forest Products Laboratory
E-mail: stan.lebow@usda.gov

*Adam Taylor**†
Professor and Wood Products Specialist
University of Tennessee
Knoxville, TN
E-mail: adamtaylor@utk.edu

(Received February 2021)

Abstract. Tyloses are extruded cell contents of adjoining parenchyma cells that result in the obstruction of vessels. The function of tyloses in live trees is uncertain, but it has been proposed that they increase the natural durability of the wood by limiting water movement and the probing of fungal hyphae. Chestnut oak (*Quercus montana*, aka *Quercus prinus*) is inconsistent in producing tyloses; an initial study indicated a wide variation in the frequency of tyloses within and between trees of chestnut oak from three different states: VA, TN, and PA. This naturally occurring variation in tylosis abundance provides an opportunity to evaluate the impact of tyloses on natural durability. In this study, samples were further examined for extractive content, rate of wetting, and natural durability, to determine if these properties were related to the prevalence of tyloses. Tylosis abundance was not related to the density or extractive content but appeared to reduce water uptake, and fungal decay in laboratory tests. The mechanism of tyloses' role in reducing decay is unclear but may include reducing water and/or fungal hyphae movement through the vessels.

Keywords: Tylosis, durability, anatomy, white oak.

INTRODUCTION

Chestnut oak (*Quercus montana* Willd., aka *Quercus prinus*) is a species of the white oak group which is common and widespread in US eastern hardwood forests. It should be noted that there has been substantial confusion regarding the taxonomy of chestnut oak, and although historically it was often referred to as *Q. prinus*, *Q. montana* is now the favored nomenclature (Carey 1992; Hardin 1979). The species is commonly used for the production of lumber, crossties, and other products (Panshin and De Zeeuw 1980). Like other white oaks, chestnut oak heartwood is considered to be naturally durable (Scheffer et al 1949). However, unlike *Quercus alba*, which receives a premium in the market because of its suitability for making barrels for aging whiskey and wine (cooperage), chestnut oak is inconsistent in forming tyloses.

A tylosis is a protrusion from an adjoining parenchyma cell that enters through a pit cavity in a vessel element wall and which partially or completely obstructs the lumen of the vessel element (Baas 1983). Tyloses are common in some species and may be associated with heartwood

* Corresponding author

Wood and Fiber Science, 53(2), 2021, pp. 126-146
https://doi.org/10.22382/wfs-2021-14

formation; however, tyloses also occur naturally in the sapwood after cavitation resulting from water stress, and may occur in sections of the stem that have been wounded or infected (De Micco et al 2016). The utilization of wood can be significantly impacted if the lumens of its vessels are completely obstructed by tyloses, eg making the wood suitable for barrels to hold liquids (tight cooperage). Tyloses also slow the drying of the wood and hinder the penetration of preservatives.

White oaks such as *Quercus alba* consistently show tyloses in all but the most recently formed vessels. Although chestnut oak is in the white oak group (genus *Quercus*, subgenus *Quercus*, section *Quercus* (Denk et al 2017)), preliminary observations indicated that there is much variation in the frequency of tyloses of chestnut oak (Fig 1). Notice the bimodality, clumping at low values, and general over-dispersion (variance > mean) indicating that there is more heterogeneity in tyloses' occurrence than would be expected under a simple count (Poisson) model. A previous analysis showed most of the variation was due to the prevalence of tyloses across the radius (within tree variation), although there was some evidence of an increase in tyloses in trees that were grown at higher elevations (between tree variation) (Taylor 2018).

White oaks, and a number of other hardwoods such as black locust, mulberry, and Osage orange that typically have tyloses, are naturally durable (Scheffer and Morrell 1998). It has been suggested that tyloses might play a role in durability by hindering the movement of fungal hyphae, water, and/or solutes (De Micco et al 2016). However, extractive composition and quantity are also associated with natural durability, and vary by species (Kirker et al 2013), so the relative importance of tyloses in durability is hard to discern. Furthermore, there are durable hardwoods that lack tyloses (eg *Swietenia mahogani*) and hardwoods with tyloses that are not durable

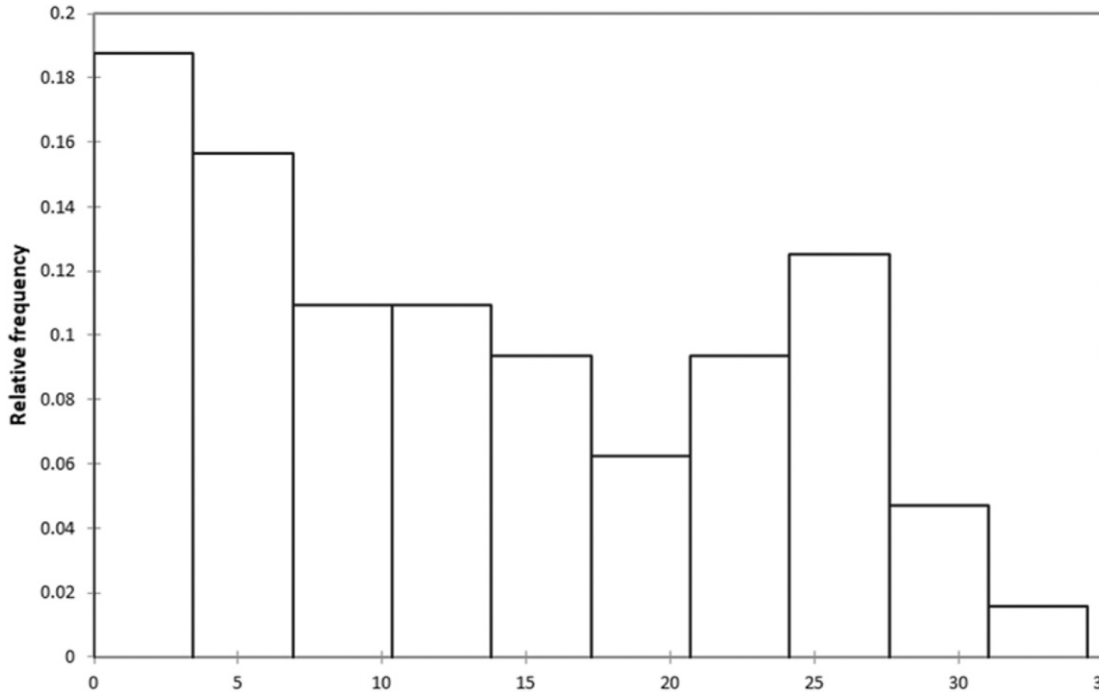

Figure 1. Preliminary measurements of the occurrence of tyloses in chestnut oak (Taylor 2018). Measurements were of number of open vessels in a 6-mm sampling circle. A total of 526 measurements were taken every 20 mm across the radius of 63 trees.

(eg *Celtis occidentalis*) (InsideWood 2004-onward).

Because chestnut oak has a wide variation in tylosis occurrence, this species should provide an opportunity to study the role of tyloses in durability. The aim of this study was to investigate the relationships among tylosis abundance, water uptake, and natural durability of chestnut oak.

MATERIALS AND METHODS

Source of Samples

The samples for this study were taken from a prior study that assessed variation of tyloses' abundance within and between trees from different states in the eastern United States (Taylor 2018). The samples for the prior study were obtained from crosscuts from the butt ends of logs delivered to sawmills in PA, VA, and TN in 2017. After cutting, the samples were dried under ambient conditions to EMC and then were resawn for tylosis examination. From the 64 available chestnut oak specimens that were examined in the previous study (Taylor 2018), 25 were selected for further sampling in this study based on their size (some were too short in length to provide sufficient material) and varying amounts of tyloses (based on wide geographical region representation).

Samples were taken from the heartwood only. Radial sections with a width of 14 mm (tangential) and a minimum height of 25 mm (longitudinal) were cut from each log cross-section specimen (Fig 2). The height of 25 mm allowed for a 3-mm cut loss to the circular saw blade kerf and an additional 2-mm margin for machining to precisely uniform dimensions. The top part of each piece (cross-section) was cut with a fine-tooth circular saw to obtain a thickness of 22 mm (longitudinal) and a smooth surface for the microscopic evaluation of the sections. The pieces were then trimmed to a length of 94 mm (radial direction). Depending on the diameter of the tree, this strip covered more or less of the total heartwood section but never included the pith (the remnant of primary growth). Subsequently, a strip measuring 14 × 96 × 5 mm (tangential × radial × longitudinal) was cut from each piece, and the remaining strip was cut into six 14-mm cubes with a band saw, and marked so the cube could be matched to the source log, and to its location in the radial strip (1-6). The whole procedure yielded 25 strips, with each of the six 14-mm square subsections marked for microscopic evaluation of tyloses' abundance, as well as 150 matching sample cubes (wood cut from immediately below) for the subsequent testing. For subsequent analyses (extractive content, water uptake, and fungal decay), the matched cube samples were stratified into groups matching the tyloses' abundance ranges: 40-60%, 61-70%, 71-80%, 81-90%, and 91-100%. These strata did not necessarily correspond to the tree the strip was taken from. Cubes were drawn roughly proportionately from each of these groups for the subsequent tests, in an effort to get a broad and similar range of tylosis prevalence in each test. Distribution of blocks from each strip to the various tests resulted in n∼25 for each test.

Figure 2. Photo of a prepared specimen sample showing the six sections marked on the strip and the six matching sample cubes. The cubes were cut from wood immediately below the strip samples (separated only by the 2 mm of wood removed by the saw blade).

Quantification of the Prevalence of Tyloses

Each of the six, 14-mm square areas on the specimen strips was examined with an Olympus ZSX10 microscope (Olympus, Tokyo, Japan). The microscopic evaluation included counting the total number of earlywood vessels and the

number of these vessels that were not sufficiently blocked by tyloses to block the penetration of light from a lamp placed underneath the (5-mm thick) sample.

In some cases, incomplete or inconsistent tylosis formation in vessel lumens complicated their precise classification as either "open" or "blocked," so categorization was somewhat subjective (Fig 3). Similarly, the definition of 'earlywood' pore was subjective; however, white oaks in general have a very large difference in pore diameter from earlywood to latewood. All observations were made by the same individual (coauthor W.R.), using a consistent setup.

Extractive Content

Extractives in wood are nonstructural components and, in the heartwood, they are assumed to provide protection against biological degradation (ie natural durability) (Taylor et al 2002). The extractive content of the samples was measured in an attempt to control for this variable.

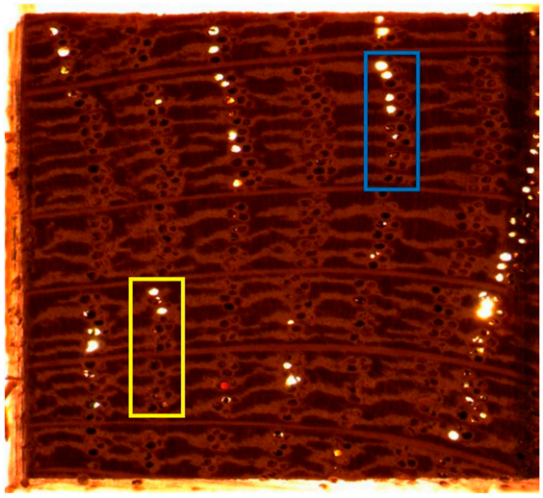

Figure 3. Photograph of one section of a specimen strip in which the blocked and open vessels were counted (10× magnification). For example, the blue section shows a total of 24 vessels, of which five were counted as "open" and 19 as "blocked." The yellow section shows a total of 18 vessels, of which two were considered "open" and 16 were considered "blocked."

The determination of the extractive amount was conducted using a modified version of ASTM standard D 1105 (ASTM 2013). Samples were ground to powder using a Retsch MM440 ball-mill (45 s, 300 Hz). Weighed powder samples were sealed within separate polyester-mesh bags (ANKOM Technologies, mesh-size of 25 microns) with an impulse heat sealer. Extractives were removed using a Soxhlet apparatus with a toluene–ethanol mixture (ratio 2:1) in the first step and 95% ethanol in the second step. Each extraction was run for at least 10 cycles, by which time the solvent ran clear. After each of the extractions, the samples were placed in a fume-hood overnight to allow residual solvent to evaporate. Finally, the samples were extracted three times in a hot-water bath (~100°C). Afterward, the samples were dried to weight equilibrium in a drying cabinet at 103°C.

The extractive content was calculated as the mass lost from each sample, with a correction for the initial wood MC and the mass of the bag.

Water Uptake

As water is necessary for fungal decay, the rate of water uptake can affect the rate of decay in short-term, standardized laboratory tests, such as that used here. Because tyloses block large-diameter cells, it is reasonable to expect that samples with more tyloses may wet more slowly, possibly influencing results from decay testing. To determine the impact of tyloses on the rate of water absorption, a test was carried out that followed a method described in standard method EN 317 (CEN 1993). This test determines the water uptake over time of samples that are completely submerged in water.

Before testing, all the samples were equilibrated to laboratory temperature and humidity conditions (~20C, 60% relative humidity [RH]). MC measurement (described in the following text) indicated an average initial MC of 10%. Sample cubes ($N = 25$) were arranged with 4 mm distance to each other so that water could touch each sample equally from all six sides. The samples

were then fixed between two grates to prevent them from floating. Each sample was completely submerged in a container filled with tap water. The samples (fixed between the grids) were placed in the container so that they were all at the same level. The samples remained submerged at 20 ± 5 mm below the water surface until they were weighed. The test was carried out at a stable room temperature of 20 ± 1°C for 63 d, and the samples were weighed every 2 h for the first 10 h of the test and after 20 h. After the first 24 h of the test, the samples were weighed approximately every 24 h. Later, the samples were weighed at longer time intervals due to the slow uptake rates at the time (25 blocks at 20 time points, with final measurement at 1508 h; one block was misplaced at 500 h, for a total of 495 measurements with the final *N* at 24).

Fungal Decay

The fungal decay resistance of the samples was determined with a soil/block test modified from the American Wood Protection Association E10 soil bottle test standard (AWPA 2016). Solid wood and powdered wood samples were tested, in an effort to control for the possible hyphae-blocking effect of the tyloses. The powdered samples were ground and sealed in bags as described earlier. The fungi species used in this project were *Gloeophyllum trabeum* (Mad-617-R, a brown rot) and *Trametes versicolor* (Mad-497, a white rot), which were first cultivated on malt extract agar. Each testing jar was filled with 60 ± 5 g of soil (MiracleGro Potting Mix), 100 ± 5 g of water, and a sapwood feeder strip of sweetgum (*Liquidambar styraciflua*). The jars were steam-sterilized (25 min at 120°C). After cooling, samples of fungus on agar were introduced to the feeder strips, and the jars were incubated for 2 wk (26°C, ~80% RH). After incubation, steam-sterilized sample blocks (45 minutes at 115°C) and bags were introduced onto the feeder strips in the jars and incubated at the same conditions. Any possible heating-induced effects on decay susceptibility and/or the tyloses were assumed to be equal for all

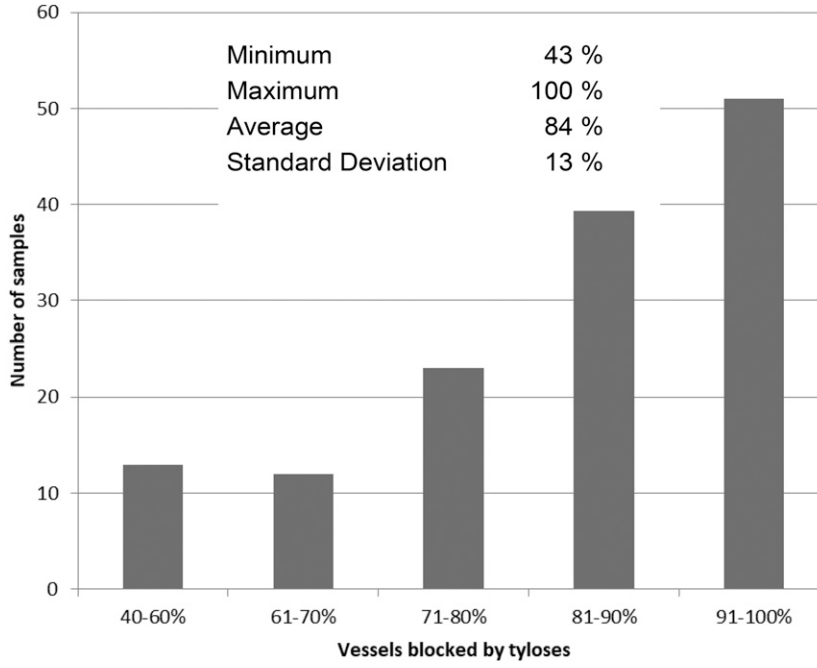

Figure 4. Histogram of the occurrence of tyloses in the chestnut oak samples.

samples. Decay-susceptible sweetgum sapwood control blocks were prepared in replicate testing jars to document if the test conditions were suitable for decay. Because of the relatively high natural durability of chestnut oak against fungal decay, the incubation period was extended to 19 wk. Post-incubation, the samples were removed from the jars, dried, and weighed. Decay was measured as mass lost from the sample, with a correction for the initial MC (and the bag, for the powdered samples).

After the first round of decay testing, another trial was run in which the test blocks were pre-wetted. The test was performed as described earlier, using blocks that had previously been used for the water uptake test, but were then pressure-treated with water and allowed to dry to approximately 40% MC before being placed in the test. This test was limited to the brown rot fungus, given that the white rot test did not perform well in the previous test.

Density and MC

The density of the samples was determined by weighing and measuring the volume of the cubic samples with calipers at equilibrium with laboratory conditions. MC was measured as the weight loss after drying to equilibrium at 103°C, relative to the oven-dry mass. For the uptake

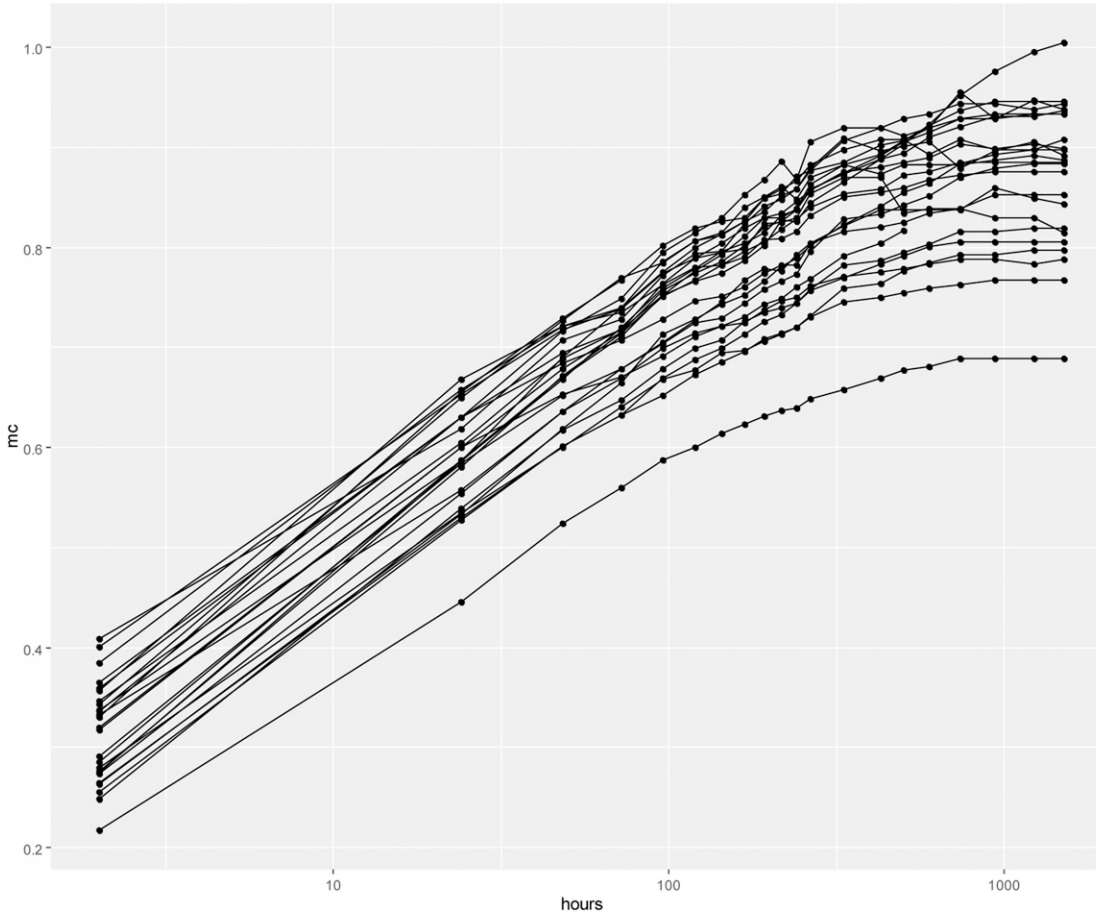

Figure 5. Spaghetti plot of observed moisture contents (dots) over time for each block on the logarithmic time scale.

measurements, air dry–specific gravity is based on the oven-dry mass divided by the volume of each block (2744 mm^3) at the start of the experiment (average MC of 10%).

Statistical Analysis

Most bivariate relationships were initially examined with simple linear correlation (simple linear regression = slr), including the coefficient of determination (R^2) and Pearson's correlation coefficient, r ($= \pm\sqrt{R^2}$). However, when assumptions for simple linear correlation were violated (ie dependent measurements, nonlinear relationships, and non-normal distributions) further analyses were carried out. To further explore how water uptake changed over hours of immersion, fraction tylosis blockage, and specific gravity, conditional plots (co-plots) were examined (Cleveland 1993). Co-plots allow the examination of bivariate relationships adjusted for other variables. The plots are a lattice plot constructed as panels of smaller plots, where each row and each column correspond to a subset of observations from third and fourth variables, respectively. For the conditioning variable that designates the rows (columns), there is a rectangular plot on the right (top) side of the lattice plot consisting of high-low boxes that indicate the range of values observed for the conditioning variable corresponding to each row (column). The subsets overlap some to provide smoother

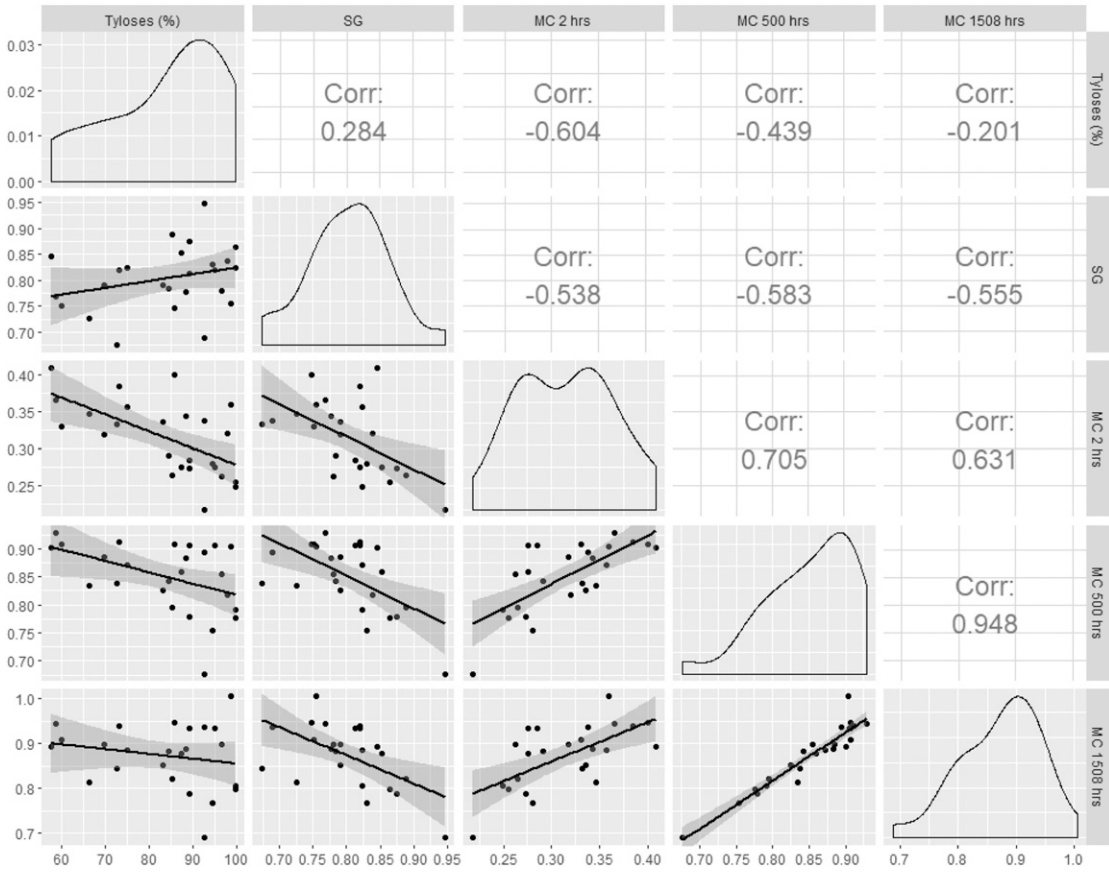

Figure 6. Scatterplots showing the Pearson correlation coefficients between the blocks' percentage of vessels with tyloses, specific gravity, and water uptake after 2, 500, and 1508 h of submersion, respectively. Note: diagonal plots are smoothed density plots. Also, note: scale changes for water uptakes (MC).

transitions. The smaller plots are scatterplots of water uptake vs hours of immersion, tyloses, or specific gravity. Water uptake was modeled using nonlinear mixed-effect models with the nlme package (version 3.1-140, Pinheiro et al 2016) in the statistical package *R* (version 3.6.1, R Core Team 2019). Further details can be found in the Appendix.

RESULTS AND DISCUSSION

Frequency of Tyloses

Overall, 84% of the 57,956 vessels observed contained tyloses. The distribution of the samples with varying tylosis frequency was skewed toward greater abundance (Fig 4).

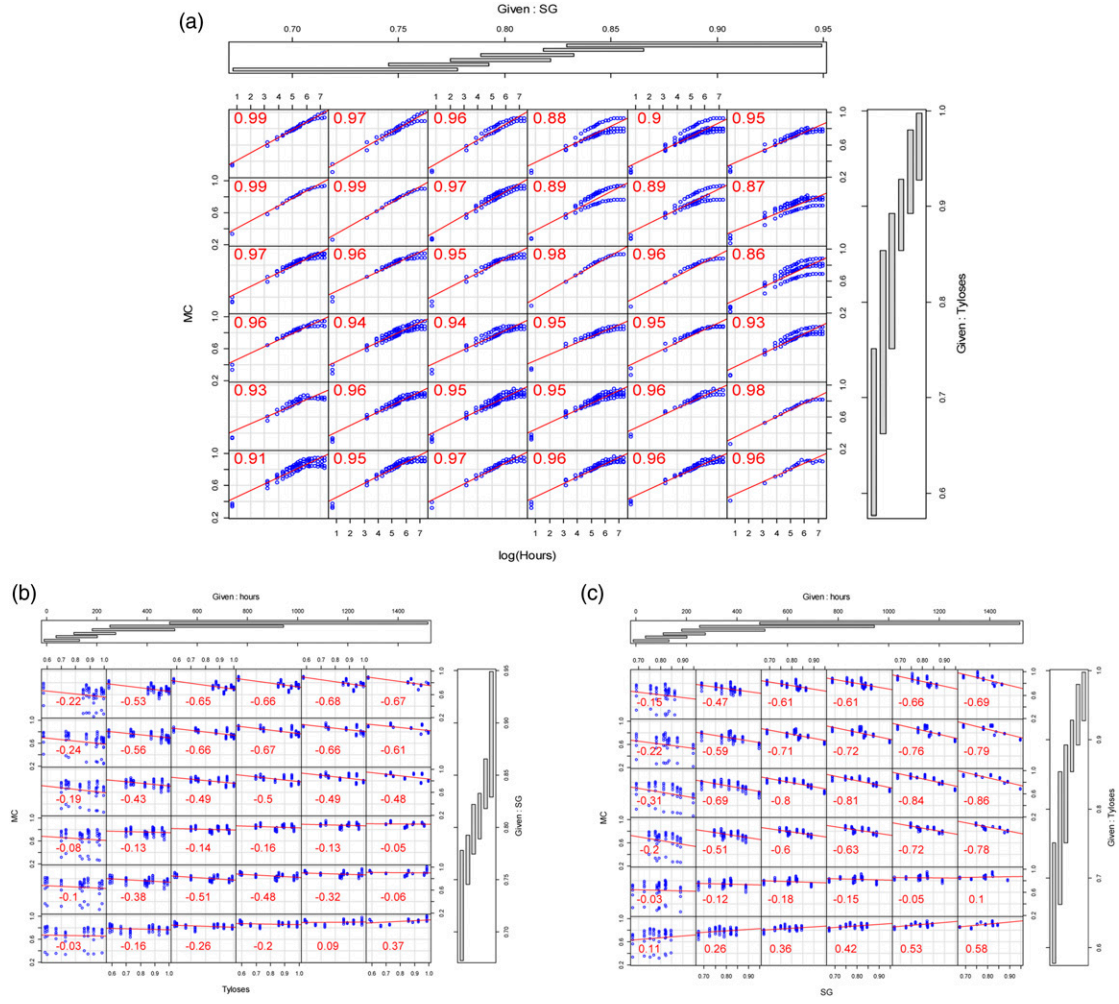

Figure 7. (a) Co-plot of water uptake vs log time conditioned on tyloses (rows) and specific gravity (columns). (b) Co-plot of water uptake vs tylosis fraction conditioned on hours of immersion (columns) and specific gravity (rows). (c) Co-plot of water uptake vs specific gravity conditioned on hours of immersion (columns) and tylosis fraction (rows). Numbers within each square are the Pearson correlation coefficient.

Water Uptake

Water uptake was expected to follow some type of asymptotic growth pattern. The effects of tyloses on that behavior were explored using simple models to estimate uptake rates, and their association with tylosis fraction. If uptake could be characterized with a single uptake rate per block, we would expect a plot of the block responses on the logarithmic scale to be linear. However, plots did not illustrate that to be the case. Figure 5 shows MC vs time, with time on the logarithmic scale, showing what initially appears to be a semilogarithmic relationship, but that the uptake rate declined further at between 100 and 500 h.

Simple bivariate relationships indicated initial water uptake was negatively correlated with the abundance of tyloses and specific gravity (Fig 6). Over time, the specific gravity relationship was maintained, but the tylosis relationship changed. Although it appears that the tyloses impeded water uptake for at least 500 h after submersion ($p = 0.02$, slr), further evaluation of the relationships was performed. Specific gravity was also negatively correlated with water uptake at 2 h (p-value < 0.01, slr; Fig 6), but specific gravity

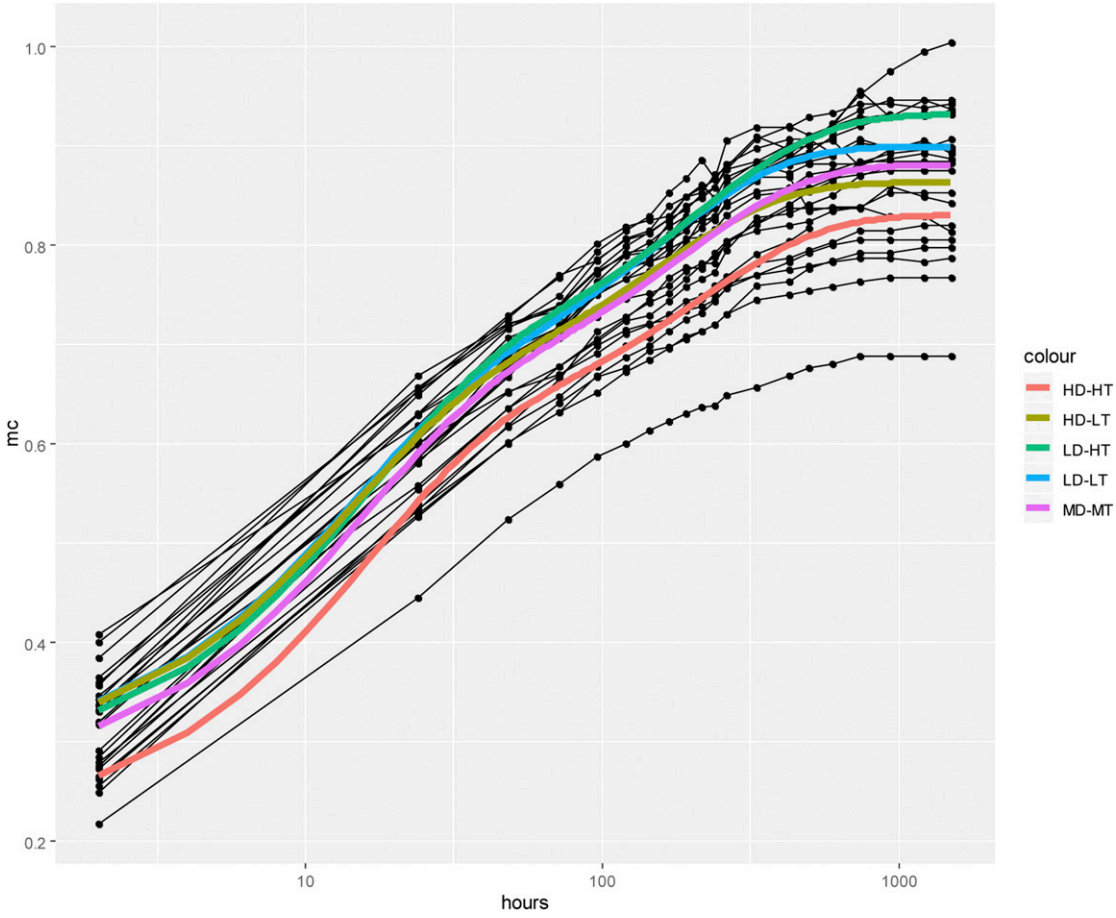

Figure 8. Model predictions based on near-low, medium, and high quartiles of observed tylosis abundance (LT = 0.75, MT = 0.87, and HT = 0.95) and specific gravity (LD = 0.75, MD = 0.80, and HD = 0.85). Black dots indicate actual observations, whereas lines connect observations for an individual block.

and tylosis prevalence did not appear to be related (p-value = 0.17, slr).

Figure 7(a)-(c) show conditional plots (co-plots) of uptake vs hours of immersion, tylosis fraction, or specific gravity as conditioned for the remaining two factors. Figure 7b shows how water uptake varied with fraction of tyloses at given intervals of immersion time (columns) and specific gravity (rows). It shows that at low specific gravities, tyloses did not appear to have a relationship with water uptake, but there was a negative relationship between tyloses and uptake at higher specific gravities. Figure 7c shows how water uptake varied with specific gravity at given intervals of immersion time (columns) and tyloses (rows). It shows there was a negative relationship between water uptake and specific gravity at higher tyloses levels. These plots indicate strong relationships over time, with a potentially interactive role between tylosis fraction and specific gravity on the influence of water uptake. An explanation for this relationship is not immediately apparent but it may be relevant to consider these potential factors 1) in addition to changes in cell wall/lumen proportion, denser oak (i.e. ring porous) wood can result from changes in the relative abundance of the latewood (faster growth = more latewood = higher average density; Panshin and DeZeeuw 1980); 2) the tyloses observed in this study were only those in the relatively low-density earlywood; 3) the tyloses may hinder vapor movement through the tyloses but it seems unlikely that tyloses would directly affect wood density, since the tylosis material present in the lumen of the pores was in the adjacent parenchyma cells (DiMicco et al. 2016). More research would be required to better understand the relationship of tyloses, density and fluxes in wood moisture content.

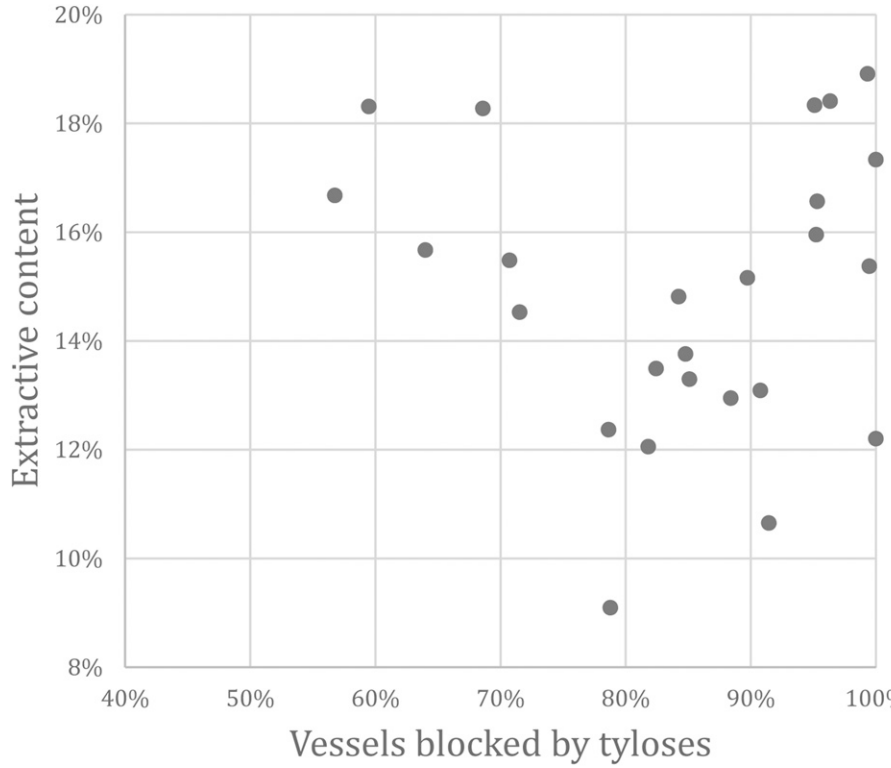

Figure 9. Tylosis occurrence and extractive contents in chestnut oak samples.

Nonlinear models that characterize asymptotic behavior as exhibited in Fig 5 were examined. Bi-exponential models are common models that capture the dominant biphasic behavior, such that can occur in two compartment systems, by partitioning a response into additive parts. They are used in a variety of fields, including pharmacokinetics, medical imaging, and chemical kinetics (Sheiner and Beal 1981; Bates and Watts 1988), and can capture the behavior like that observed in Fig 5. The following bi-exponential model form was fit to the data:

$$\mathrm{MC} = \mathrm{MC}_0 + \Delta\mathrm{MC}_1 * (1 - \exp[-\exp\{\alpha_1\} t]) + \Delta\mathrm{MC}_2 * (1 - \exp[-\exp\{\alpha_1\} t]),$$

where MC_0, $\Delta\mathrm{MC}_1$, $\Delta\mathrm{MC}_2$, and α_1 and α_2 are the model parameters, and t is the time (hours of immersion). Model development and evaluation details are given in the Appendix. The final model estimated an interactive role between tylosis fraction and specific gravity, with predictive behavior similar to that of the bivariate and conditional plots of Figs 6 and 7. Figure 8 illustrates predictions from the model overlaid on the observed water uptake curves. In particular, the model indicated water uptake *rates* were primarily dependent on tylosis abundance, whereas initial and final moisture *contents* were a function of both tyloses and specific gravity, respectively.

Extractive Content

On average, the extractive contents were about 15%, which is in the range of extractive content values for heartwood of white oak species (Taylor et al 2011). The extractive content was not related to the abundance of tyloses (p-value = 0.87, slr; p-value = 0.68, test of Spearman's ρ; Fig 9).

Resistance to Decay

After 19-wk of exposure, good weight losses were achieved in the brown rot test; the white rot test was less successful (Table 1). The fungal decay test showed some evidence ($R^2 = 0.15$, p-value = 0.07, slr) that an increased tyloses occurrence in vessels impeded (brown rot) decay of the chestnut oak wood cubes. Powdered samples did not show this correlation ($R^2 = 0.01$, p-value = 0.72), while still showing a significant reduction in mass due to decay.

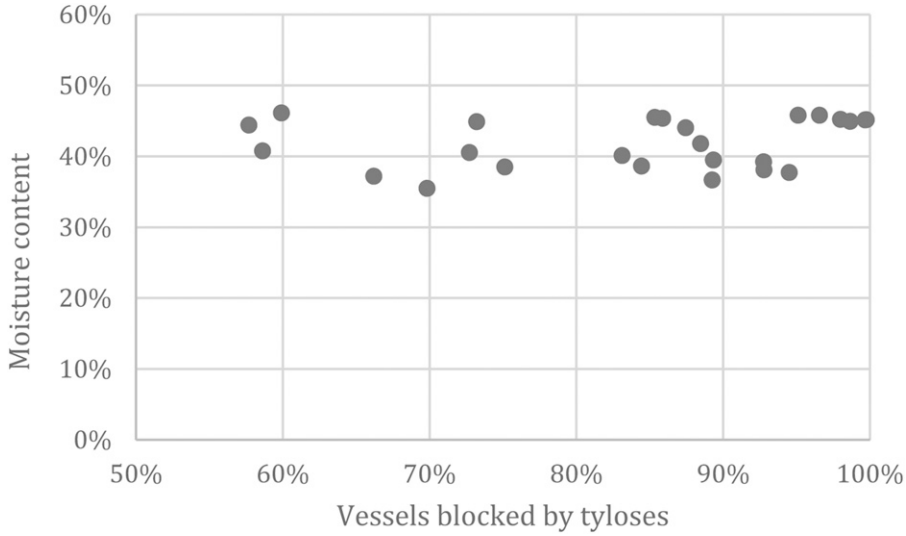

Figure 10. MC of pre-wetted oak cubes when placed in the decay test bottles.

Table 1. Decay data (percent mass loss) after 19 wk exposure in soil bottle test.

	Brown rot (*Gloeophyllum trabeum*)			White rot (*Trametes versicolor*)		
	Control blocks (%)	Oak blocks (%)	Oak powder (%)	Control blocks (%)	Oak blocks (%)	Oak powder (%)
Minimum	0.3	0.6	−1.3	−0.4	0.7	−2.1
Maximum	66.4	58.4	67.4	28.5	27.0	3.2
Average	43.7	24.1	35.5	7.4	9.4	−0.8
Standard deviation	32.8	18.5	25.6	11.9	8.2	1.3

Decay of Pre-wetted Blocks

The pre-wetted samples had an average MC of 42% when placed in the soil bottles, and their initial MC was not related to the abundance of tyloses (p-value = 0.37, slr; Fig 10).

Weight loss in the pre-wetted blocks was low on average (4%), compared with that in the previous brown rot decay tests (24%). Control block decay was consistently high (42-72%), suggesting that test conditions were suitable. The results suggest that the 42% initial MC of the oak blocks was not suitable, despite being within the reported optimal range for decay (Zabel and Morrell 2020). Void volume is relatively low in dense wood samples such as these. Thus, whereas free water would be abundant at 42% MC, low free oxygen may be limiting, especially if that free water was concentrated in lumens without tyloses.

There was some evidence that pre-wetted blocks with more tyloses were less susceptible to decay (p-value = 0.08, slr; Fig 11) but only after two outliers were removed from the calculation. If the

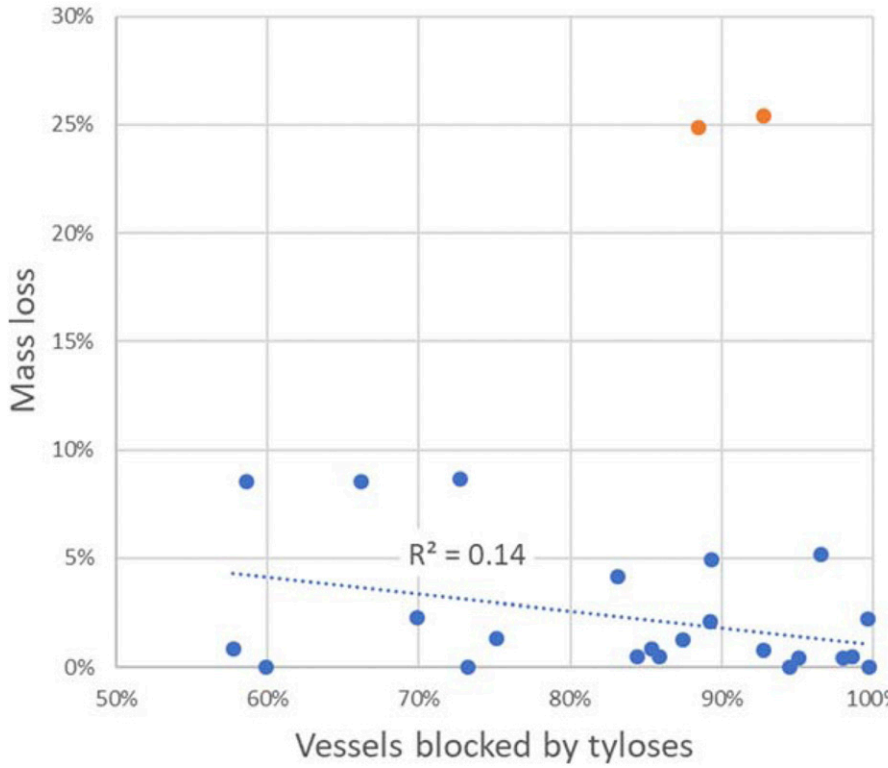

Figure 11. Decay of pre-wetted chestnut oak blocks after 19 wk exposure to *Gloeophyllum trabeum.* Two outliers (orange) were excluded from the calculations.

outliers were not removed, there was no relationship between mass loss and tyloses

Extractives are often thought to be of primary importance in wood natural durability. In white oaks and other durable hardwoods, reports suggest that phenolic components contribute to durability (Aloui et al 2004; Guilley et al 2004; Hart and Hillis 1972; Taylor et al 2011). One study has also reported that methanol extracts of *Quercus montana* stem and leaf tissue exhibit antimicrobial activity against bacteria and mold fungi (Subhashini et al 2016).

Although our study did not test the role of extractives in the durability of *Quercus montana*, we did find evidence that tylosis abundance was associated with increased decay resistance but not with extractive content, suggesting that the tyloses themselves play a role in durability. However, it is difficult to discern if the decay-impeding effect of tyloses is due to reduced water permeability, physical blocking of fungal hyphae, or some other effect. Tyloses impeded the wetting of the blocks used in this study, and this effect was surprisingly long-lasting. This suggests that tyloses can prevent wood from being wet enough to support decay, at least for a time. However, under continuous immersion, the wood samples eventually absorbed enough moisture to support decay, regardless of tylosis abundance. This suggests that tyloses may play a different role in limiting decay for wood exposed to intermittent wetting (eg decking), than in the durability of wood in long-term soil exposure (eg fence posts) or, especially, in the living tree.

Wood powder decay rates did not appear to differ according to whether they came from solid wood with more or fewer tyloses, again providing evidence for the decay-impeding effect of the tyloses themselves. However, grinding the wood to powder would reduce any potential wetting-rate *and* hyphae-blocking effects of the tyloses. A decay test with pre-wetted blocks was performed in an attempt to control for the slow wetting rate of tylosis-rich samples; the results were only suggestive: decay was slightly less in wood with more tyloses, but overall decay levels were low and the data contained outliers.

CONCLUSIONS

The function of tyloses in live trees is uncertain, but it has been proposed that they increase the natural durability of the wood by limiting water movement and the probing of fungal hyphae. Chestnut oak (*Quercus montana*) provides an opportunity to study the impact of tyloses on wood durability, due to this species' inconsistent tylosis formation. Data in this article provide evidence that tyloses contribute to fungal decay resistance; samples with greater tylosis abundance experienced reduced decay losses even though tyloses were not correlated with the extractive content. Tyloses slowed the water uptake rate of small samples, suggesting that tyloses may affect the movement of water for decay. However, tyloses may also impede the movement of fungal hyphae through the lumen, which would otherwise be an open pathway; in this study, there was some evidence that tyloses were associated with reduced decay, even in samples that had been pre-wetted to MC levels suitable for fungal activity. Strong interactive effects between specific gravity and tyloses were detected in the water uptake models and could be impacting the decay results. Further study is needed to confirm some of the findings suggested by this dataset, and to separate the relative importance of water-impeding and hyphae-blocking effects of tyloses.

REFERENCES

Aloui F, Ayadi N, Charrier F, Charrier B (2004) Durability of European oak (*Quercus petraea* and *Quercus robur*) against white rot fungi (*Coriolus versicolor*): Relations with phenol extractives. Holz Roh Werkst 62:286-290.

ASTM (2013) SD-96 standard test method for preparation of extractive free wood. American Society for Testing and Materials, West Conshocken, PA.

AWPA (2016) Laboratory method for evaluating the decay resistance of wood-based materials against pure basidiomycete cultures: Soil/block test. Standard E10-16. American Wood Protection Association, Birmingham, AL.

Baas P (1983) A new multilingual glossary of terms used in wood anatomy. IAWA Bulletin. New Series 6:83.

Bates DM, Watts DG (1988) Nonlinear regression analysis and its applications. John Wiley & Sons. New York, NY. 365 pp.

Carey JH (1992) *Quercus michauxii*, *Q. montana*. Fire Effects Information System, [Online]. U.S. Department of Agriculture, Forest Service, Rocky Mountain Research Station, Fire Sciences Laboratory, Missoula, MT. https://www.fs.fed.us/database/feis/plants/tree/quespp3/all.html (23 July 2020).

CEN (1993) EN 317 Particleboards and Fibreboards—Determination of Swelling in Thickness after Immersion in Water. CEN, Brussels, Belgium.

Cleveland WS (1993) *Visualizing Data*. AT&T Bell Laboratories, Lafayette, IN.

De Micco V, Balzano A, Wheeler EA, Baas P (2016) Tyloses and gums: A review of structure, function and occurrence of vessel occlusions. IAWA J 37:186-205.

Denk T, Grimm GW, Manos PS, Deng M, Hipp AL (2017) An updated infrageneric classification of the oaks: Review of previous taxonomic schemes and synthesis of evolutionary patterns. *Oaks physiological ecology. Exploring the functional diversity of genus* Quercus *L.* Springer.

Dexter AR, Czyz EA, Richard G, Reszkowska A (2008) A user-friendly water retention function that takes into account of the textural and structural pore spaces in soil. Geoderma 143:243-253.

Guilley E, Charpentier JP, Ayadi N, Snakkers G, Nepveu G, Charrier B (2004) Decay resistance against *Coriolus versicolor* in sessile oak (*Quercus petraea* Liebl.): Analysis of the between-tree variability and correlations with extractives, tree growth and other basic wood properties. Wood Sci Technol 38:539-554.

Glass SV, Boardman CR, Zelinka SL (2017) Short hold times in dynamic vapor sorption measurements mischaracterize the equilibrium moisture content of wood. Wood Sci Technol 51:243-260.

Hardin JW (1979) *Quercus prinus* L. nomen ambiguum. Taxon 28(4):355-357.

Hart JH, Hillis WE (1972) Inhibition of wood-rotting fungi by ellagitannins in the heartwood of *Quercus alba*. Phytopathology 62:620-626.

InsideWood (2004-onwards). Published on the Internet. http://insidewood.lib.ncsu.edu/search (15 June 2020).

Kirker GT, Blodgett AB, Arango RA, Lebow PK, Clausen CA (2013) The role of extractives in naturally durable wood species. Int Biodeterior Biodegradation 82:53-58.

Kohler R, Duck R, Ausperger B, Alex R (2003) A numeric model for the kinetics of water vapor sorption on cellulosic reinforcement fibers. Composite Interfaces 10(2-3): 255-276.

Panshin AJ, De Zeeuw C (1980) Textbook of wood technology, 4th edition. McGraw-Hill, New York, NY.

Pinheiro JC, Bates DM (2000) Mixed-effects models in S and S-PLUS. Springer-Verlag New York Inc., New York, NY. 528 pp.

Scheffer TC, Englerth GH, Duncan CG (1949) Decay resistance of seven native oaks. J Agric Res 78:129-152.

Scheffer TC, Morrell JJ (1998) Natural durability of wood: A worldwide checklist of species. Forest Research Laboratory, Oregon State University, Research Contribution 22. 58 pp.

Subhashini S, Maleeka Begum SF, Rajesh G (2016) Antimicrobial characterisation combining spectrophotometric analysis of different oak species. Int J Herb Med 4: 32-35.

Sheiner LB, Beal SL (1981) Evaluation of methods for estimating population pharmacokinetic parameters II. Biexponential model and experimental pharmacokinetic data. J Pharmacokinet Biopharm 9(5):635-651.

Taylor AM (2018) Tyloses in chestnut oak. Poster presented at the New Phytologist Symposium. New Phytologist Foundation, Lake Tahoe, CA. https://www.newphytologist.org/symposia/42 (15 June 2020).

Taylor AM, Gartner BL, Morrell JJ (2002) Heartwood formation and natural durability-a review. Wood Fiber Sci 34(4):587-611.

Taylor AM, Labbé N, Noehmer A (2011) NIR-based prediction of extractives in American white oak heartwood. Holzforschung 65:185-190.

Thybring EE, Boardman CR, Glass SV, Zelinka SL (2019) The parallel exponential kinetics model is unfit to characterize moisture sorption kinetics in cellulosic materials. Cellulose 26:723-735.

Zabel RA, Morrell JJ (2012) Wood microbiology: Decay and its prevention. Academic Press, New York, NY.

APPENDIX

STATISTICAL ANALYSIS

Statistical Model of Water Uptake

The oak water uptake was expected to follow some type of asymptotic growth pattern, and it was desired to determine whether blockage by tyloses had any influence on that behavior. Simple plots showed this not to be the case.

Bi-exponential models are common models that capture dominant biphasic behavior, such that it can occur in two compartment systems, by partitioning a response into additive parts. They are used in a variety of fields, including pharmacokinetics, medical imaging, water retention in soils, and chemical kinetics (eg Sheiner and Beal 1981; Bates and Watts 1988; Dexter et al 2008) and can capture behavior like that in Fig 5. The following bi-exponential model form was fit to the data:

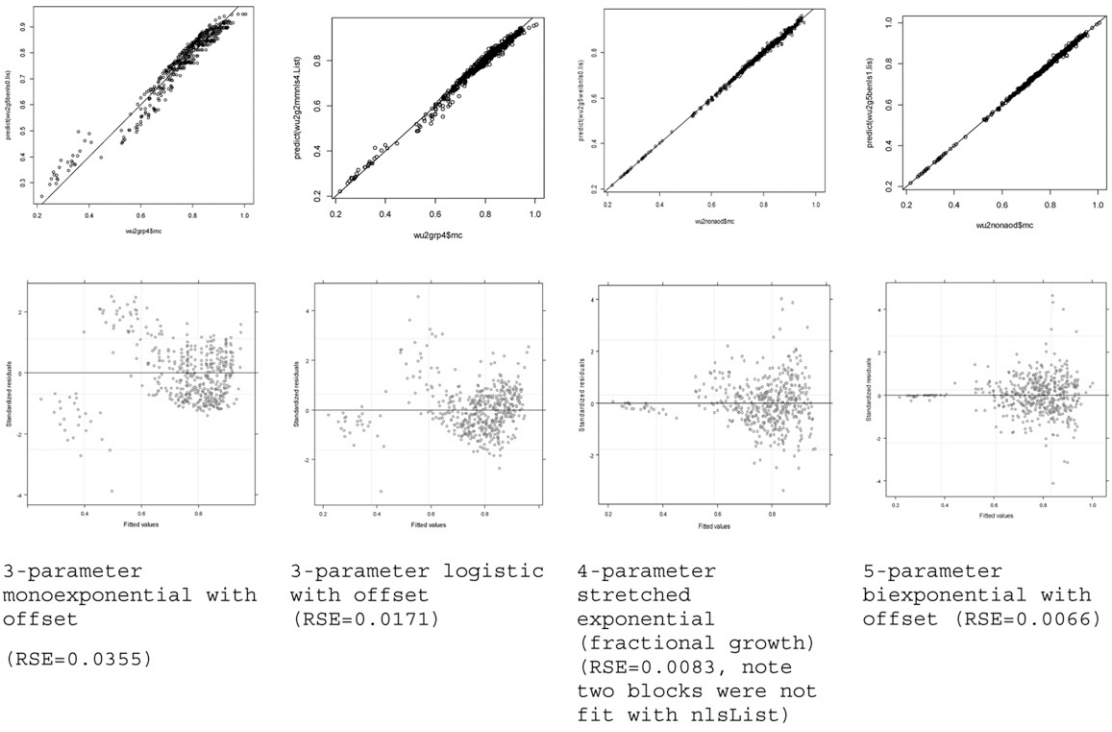

Figure A1. Separate nonlinear fits to each block's water uptake over time.

$$\mathrm{MC} = \mathrm{MC}_0 + \Delta\mathrm{MC}_1{*}(1 - \exp[-\exp\{\alpha_1\}t]) + \Delta\mathrm{MC}_2{*}(1 - \exp[-\exp\{\alpha_1\}t])$$

where MC_0, $\Delta\mathrm{MC}_1$, $\Delta\mathrm{MC}_2$, and α_1 and α_2 are the model parameters and t is the time (hours).

The model is equivalent to what is known as a five-parameter bi-exponential model and is commonly expressed in the re-parameterized form $Y = c + a_1{*}\exp(-\mathrm{b}_1{*}t) + a_2{*}\exp(-\mathrm{b}_2{*}t)$, where $c = \mathrm{MC}_0 + \Delta\mathrm{MC}_1 + \Delta\mathrm{MC}_2$ is the asymptote, $a_1 = -\Delta\mathrm{MC}_1$ and $\mathrm{a}_2 = -\Delta\mathrm{MC}_2$ are scale parameters, and the b's and exp(α)'s are equivalent rate parameters. Note that in fitting the model, the exp(α)s are constrained to positivity and $\alpha_1 > \alpha_2$ for identifiability with the first exponential term then characterizing a "faster" uptake "compartment" and the second characterizing a "slower" uptake "compartment."

This model form is also known as the parallel exponential model (Kohler et al 2003; Glass et al 2017; Thybring et al 2019) and has been used extensively more recently for modeling the dynamic vapor sorption behavior to estimate EMC. Glass et al (2017) critically evaluated this model for dynamic vapor sorption and conclude it is not appropriate for that purpose, primarily because the behavior of sorption/desorption seems to change even further as time progresses (in a functional way), indicating that more exponential components (parameters) are necessary to capture the behavior and/or another model form should be used. However, we are using the model from a more empirical perspective of a different water uptake process and trying to balance the bias/variance trade-off in model development to better understand tyloses' blockage of water sorption.

Water uptake data were collected repeatedly over time for 25 individual oak blocks, with each individual block having a fractional measure of tylosis abundance and specific gravity (covariates measured at the subject level). With repeated measurements exhibiting nonlinear behavior over

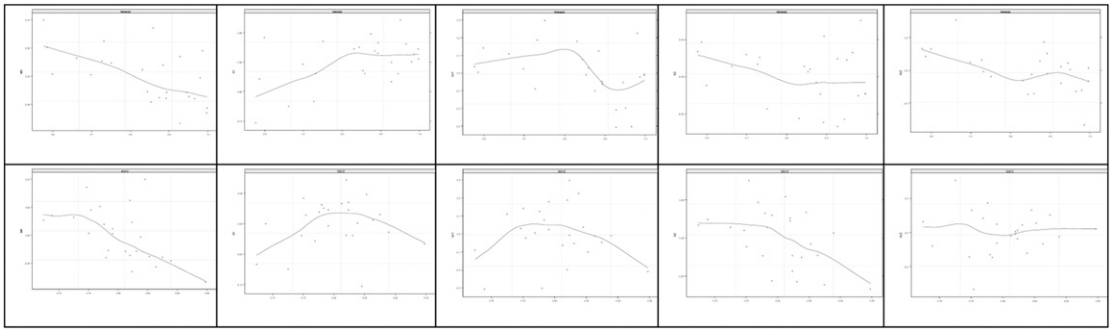

Figure A2. Predicted random effects from a bi-exponential model, and their association with tylosis fraction (top row) and specific gravity (bottom row) for each of the model parameters (columns left to right represent MC_0, ΔMC_1, ΔMC_2, and $\ln(\alpha_1)$ and $\ln(\alpha_2)$, respectively).

time, two basic stepwise approaches were used for the model building following Pinheiro and Bates (2000), and both resulted in similar conclusions about the final model form. Uptake was modeled using nonlinear least squares and nonlinear mixed-effect models with the nlme package (version 3.1-140, Pinheiro et al 2016) in the statistical package R (version 3.6.1, R Core Team 2019).

In the first approach, each individual block's water uptake was modeled following one of four asymptotic regression forms to capture the blocks' behavior, a mono-exponential form with an offset, a logistic form with an offset, a stretched exponential form (similar to mono-exponential, but allows fractional time, Weibull form), and the bi-exponential form with an offset. Separate nonlinear fits for each block's water uptake were fit with the nlsList function in the nlme package. They are compared in the plots in Fig A1, with the predictive ability and residual pattern indicating the model with the bi-exponential form captures the individual block's water uptake behavior better statistically. The bi-exponential model resulted in an 80% reduction in the overall residual standard error from a mono-exponential model form. The Weibull form (stretched exponential) also appears reasonable, but still has some patterns in the residuals.

To investigate if whether tylosis abundance and/or specific gravity can be incorporated as covariates into the model to explain individual parameter estimates and increase the information content of the model, plots of parameter estimate by blocks as ordered by either percent tyloses or specific gravity (not shown). From nonoverlapping intervals in the plots, it appears that the individual blocks have differing estimates for some of the parameters, and that in some cases, the relationship with tyloses and/or specific gravity seems to follow a general pattern of increasing or decreasing. Simple regressions of the parameter estimates against tylosis abundance were significant for four of the five parameters, indicating the potential of tyloses to be a helpful covariate (MC_0 = M0: $R^2 = 0.32$, $p = 0.0031$; ΔMC_1 = A1: $R^2 = 0.30$, $p = 0.0045$; $\ln(\alpha_1)$ = lrc1: $R^2 = 0.28$, $p = 0.0067$; ΔMC_2 = A2: $R^2 = 0.15$, $p = 0.0581$; $\ln(\alpha_2)$ = lrc2: $R^2 = 0.38$, $p = 0.0010$). Specific gravity also may be helpful as a covariate as two of five parameters are associated with it (MC_0 = M0: $R^2 = 0.31$, $p = 0.0042$; ΔMC_2 = A2: $R^2 = 0.28$, $p = 0.0067$; others $p > 0.35$). This suggests that a model that also includes a fixed effect for tyloses and/or specific gravity, plus random effects for blocks, may be more appropriate for inference and prediction purposes.

Second, following another approach as outlined in Pinheiro and Bates (2000), the aforementioned bi-exponential model was set as a base model to capture overall parameter estimates, and random effects were added to each model parameter to capture the individual block behavior. This behavior then could be evaluated to determine if the specific gravity or percent tyloses for each block was associated with that block's random effect deviation

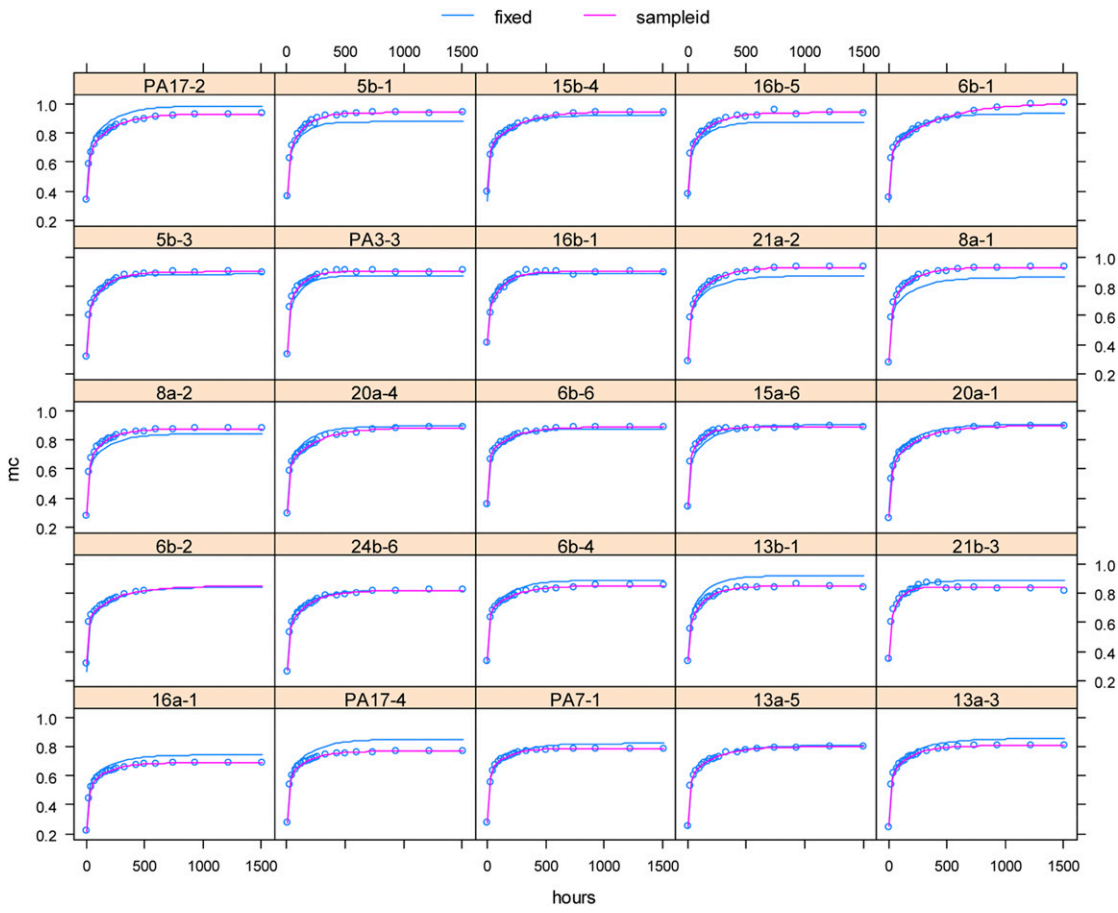

Figure A3. Oak block–specific (sampleid-magenta line) and population average (fixed-blue line)-predicted water uptake. The circle markers are the observed MC.

from the overall population parameter estimates. Thus, each block's random effect deviation associated with the parameters MC_0, ΔMC_1, ΔMC_2, and $\ln(\alpha_1)$ and $\ln(\alpha_2)$ were considered as linear functions of the block's specific gravity or tylosis fraction. Figure A2 shows how the random effects vary with tylosis fraction (top row) and specific gravity (bottom row), with similar parameter implications as were indicated in the individual models approach, that tylosis abundance and specific gravity have some relationship with the water uptake behavior.

Therefore, to evaluate how tylosis fraction and/or specific gravity affects water behavior uptake following a bi-exponential model frame, a series of models were developed that added the covariates to each of the model parameters. Two separate models with either just the covariate tylosis fraction or just the covariate specific gravity were added to each of the model parameters:

$$\begin{aligned} MC = {} & MC_0 + \beta_0 x + (\Delta MC_1 + \beta_1 x) \\ & * (1 - \exp(-[\exp\{\alpha_1 + \lambda_1 x\}]t)), \\ & + (\Delta MC_2 + \beta_2 x) \\ & * (1 - \exp(-[\exp\{\alpha_2 + \lambda_2 x\}]t)), \end{aligned}$$

where x represents the fraction of tyloses or, separately, specific gravity; also, random effects were also included to capture the remaining deviations from the population parameters. To determine the joint impact of covariates, the following model was also considered:

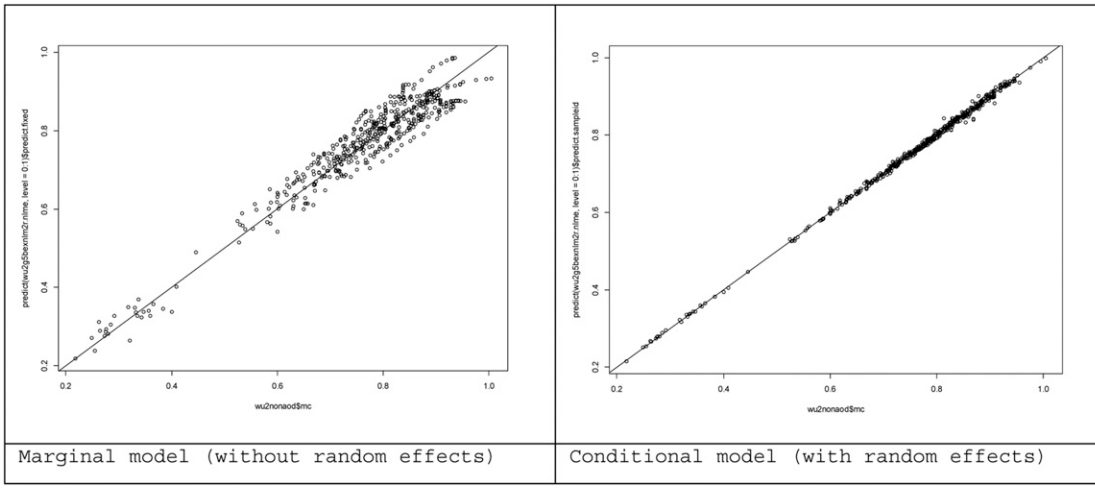

Figure A4. Water uptake predictions from the population (marginal) model (left) and the block-specific (conditional) model.

$$\begin{aligned} MC = {} & MC_0 + \beta_{01}x_1 + \beta_{02}x_2 \\ & + (\Delta MC_1 + \beta_{11}x_1 + \beta_{12}x_2) \\ & * (1 - \exp(-[\exp\{\alpha_1 + \lambda_{11}x_1 + \lambda_{12}x_2\}]t)), \\ & + (\Delta MC_2 + \beta_{21}x_1 + \beta_{22}x_2) \\ & * (1 - \exp(-[\exp\{\alpha_2 + \lambda_{21}x_1 + \lambda_{22}x_2\}]t)) \end{aligned}$$

where x_1 represents the fraction of tyloses and x_2 represents the specific gravity; also, random effects were also included to capture the remaining deviations from the population parameters. Finally, an extension of this model was considered that added to each parameter set another term for the interaction of tylosis fraction and specific gravity (x_1*x_2). This extended model can then be reduced (as determined by parameter significance) and is given by

$$\begin{aligned} MC = {} & MC_0 + \beta_{01}x_1 + \beta_{02}x_2 + \beta_{0,1*2}x_1x_2 \\ & + (\Delta MC_1 + \beta_{11}x_1) \\ & * (1 - \exp(-[\exp\{\alpha_1 + \lambda_{11}x_1\}]t)), \\ & + (\Delta MC_2 + \beta_{22}x_2) \\ & * (1 - \exp(-[\exp\{\alpha_2 + \lambda_{21}x_1\}]t)). \end{aligned}$$

The series of models are summarized in Table A1.

Comparison of the models by Akaike's information criteria (AIC) and Bayesian information criteria (BIC) shows the model with tylosis fraction offers improvement over a null model or a model with just specific gravity as a covariate. Based on the initial hypotheses of the experiment, however, neither the model with interactions nor a specific reduced model was envisioned. The individual fits have the lowest AIC, but not BIC, indicating that further modeling could potentially improve fit, but was not attempted at this point as it could be due to an unknown factor.

The aforementioned reduced model was arrived at following a stepwise procedure starting with the full model with tyloses, SG, and their interaction, and then eliminating covariate terms in a backward stepwise fashion based on their Wald tests. The final model is given in Table A2.

Figure A3 shows the model predictions of what are called the marginal population, or the "fixed" portion of the model (the blue line), and the conditional block specific, or "sampleid," portion of the model (pink line). The model still includes random effects, but their estimates are reduced from the model without the covariates. The conditional model includes predicted random effects, whereas the marginal model sets them to zero. Overall, the marginal model has an approximate $R^2 = 0.928$, and the conditional model has an approximate $R^2 = 0.998$ (Figures A3 and A4; note that a model without any covariates (just the bi-exponential form and random effects to

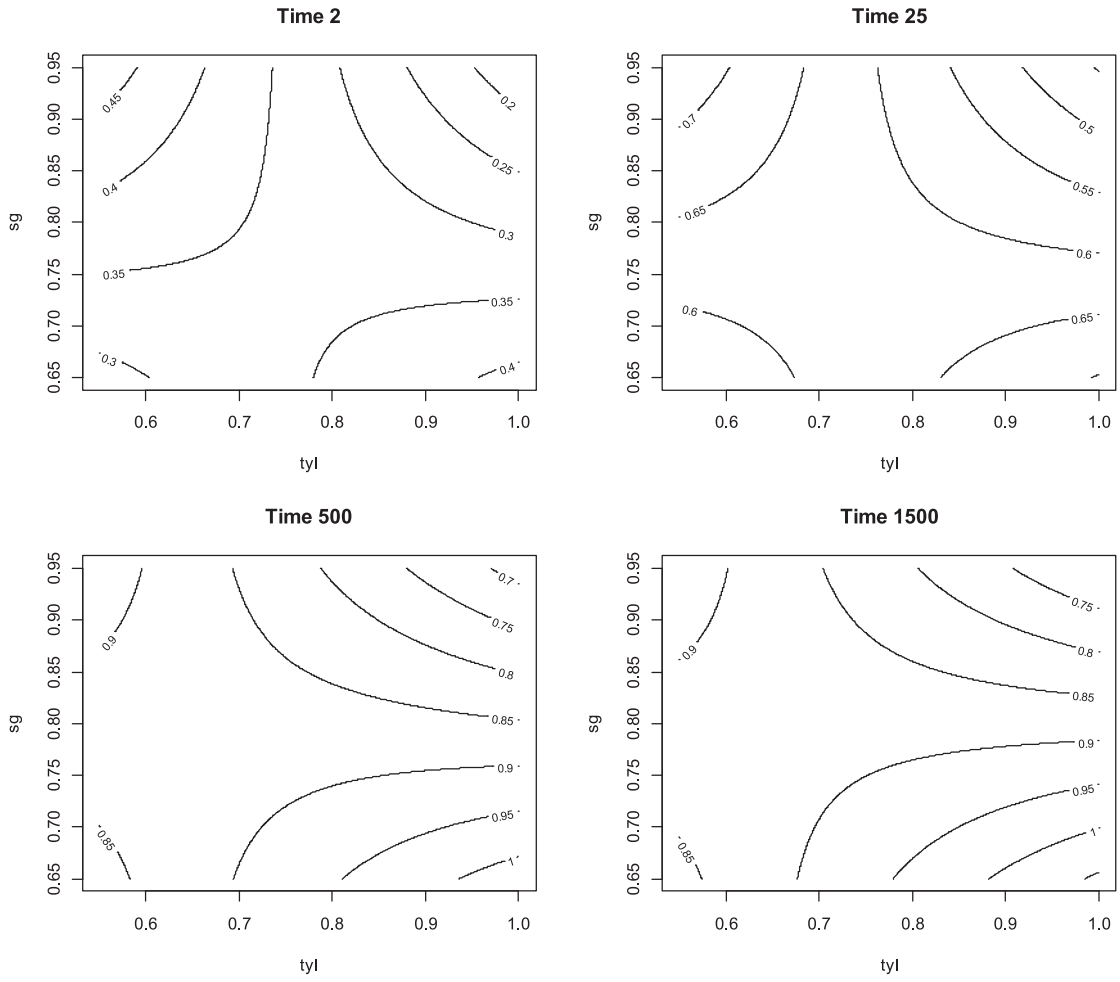

Figure A5. Contour plots of predicted MC at various times (2, 25, 500, and 1500 h) across the range of tyloses (*x*-axis) and specific gravity (*y*-axis) observed in the study (see contour plots with color gradients at the end of report).

capture block variability) had approximate R^2's of 0.828 and 0.998, for marginal and conditional models, respectively—thus, we see an improvement in the marginal model when we include the covariates, which is what we expect with helpful covariates). Figure 8 overlays several model predictions across time (from the fixed portion of the model) on the observed block moisture contents.

Table A2 below contains a brief description of the model parameter estimates and their standard errors for the bi-exponential model that includes tylosis fraction and specific gravity as covariates. In the table, *p*-values for those parameter estimates associated with tyloses, ie the parameters β_{01}, $\beta_{0,1*2}$, β_{11}, λ_{11}, and λ_{21}, indicate if the tylosis fraction is helpful for modeling that particular portion of the uptake response. Besides, the initial offset (through the parameters β_{02}, $\beta_{0,1*2}$), specific gravity influences the portion associated with ΔMC_2 = A2, through the parameter β_{22}, where the tylosis fraction does appear not to help.

From the estimates in Table A2, we can infer that tyloses ($\hat{\beta}_{01} = 2.4181,\ p = 0.0002$), specific gravity ($\hat{\beta}_{02} = 2.4462,\ p = 0.0004$), and their interaction ($\hat{\beta}_{0,1*2} = -3.2622,\ p = 0.0001$)

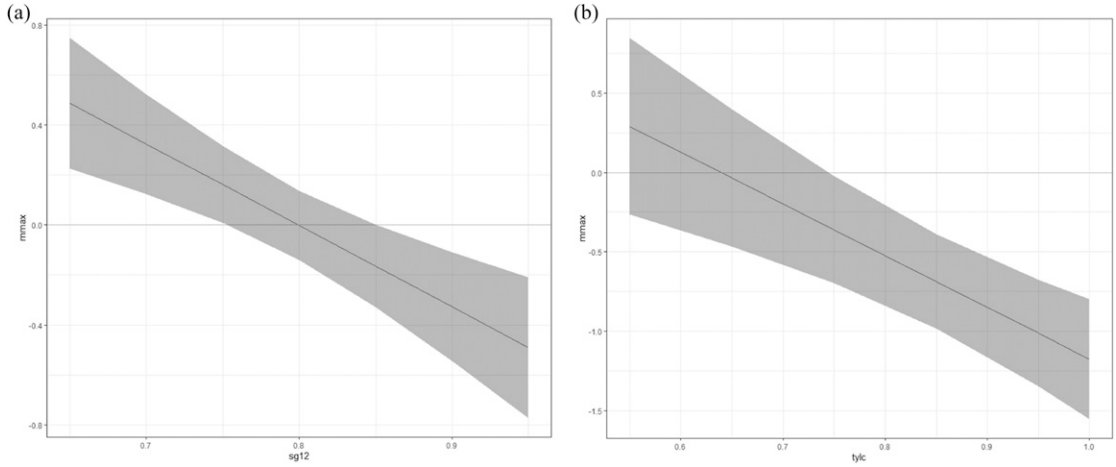

Figure A6. (a)-(b). Asymptotic coefficient estimates and confidence intervals as time approaches infinity.

influence the initial uptake. Tyloses appear to slow the uptake rate in the "faster" compartment ($\hat{\lambda}_{11} = -0.7808,\ p = 0.0140$), slow the uptake rate in the "slower" compartment ($\hat{\lambda}_{21} = -1.5636,\ p = 0.0002$), but increase the uptake range over which the "faster" compartment operates ($\hat{\beta}_{11} = 0.1900,\ p = 0.0013$). The specific gravity appears to decrease the uptake range of the "slower" compartment ($\hat{\beta}_{22} = -0.3609,\ p = 0.0040$). Figure A5 shows contour plots of predicted MC after 2, 25, 500, and 1500 h for the ranges of tyloses and specific gravity observed in the study. The plots capture the apparent interaction visible in the conditional plots in Fig 7(b)-(c).

Furthermore, by setting time to infinity and rearranging the terms in the model, we can determine how tylosis fraction hinders the total amount of wetting across a range of specific gravities (the asymptote as a function of tyloses). The model reduces to

$$\mathrm{MC} = \mathrm{MC}_0 + \Delta\mathrm{MC}_1 + \Delta\mathrm{MC}_2 + (\beta_{01} + \beta_{11} + \beta_{0,1*2}x_2)x_1,$$

Table A1. Bi-exponential models fit to the water uptake data. Models were fit with maximum likelihood for comparison of AIC and BIC, with low values indicating a better model fit.

Model	Number of parameters	Residual standard error	AIC	BIC
Null model (no covariates), no random effects	5	0.0587	−1394.70	−1369.48
Null model (no covariates), random effects for each parameter	11	0.0067	−3062.88	−3016.63
Tyloses covariate, random effects	16	0.0066	−3090.02	−3022.75
SG covariate, random effects	16	0.0067	−3069.69	−3002.42
Tyloses and SG covariates, random effects	21	0.0066	−3094.12	−3005.82
Tyloses, SG, and their interaction, random effects	26	0.0066	−3105.29	−2995.97
Reduced model with either tyloses or SG covariate, random effects	18	0.0066	−3110.52	−3034.83

AIC, Akaike's information criteria; BIC, Bayesian information criteria.

Table A2. Bi-exponential model parameter estimates and standard errors as fit by restricted maximum likelihood.

Model parameter	Estimate	Standard error	Degrees of freedom	*t*-value	*p*-value
MC_0	−1.5240	0.5419	459	−2.81	0.0051
β_{01}	2.4181	0.6340	459	3.81	0.0002
β_{02}	2.4462	0.6860	459	3.57	0.0004
$\beta_{0,1*2}$	−3.2622	0.7983	459	−4.09	0.0001
ΔMC_1	0.1945	0.0498	459	3.90	0.0001
β_{11}	0.1900	0.0586	459	3.24	0.0013
α_1	−1.9737	0.2734	459	−7.22	<0.0001
λ_{11}	−0.7808	0.3166	459	−2.47	0.0140
ΔMC_2	0.5442	0.1005	459	5.41	<0.0001
β_{22}	−0.3609	0.1248	459	−2.89	0.0040
α_2	−3.8493	0.3516	459	−10.95	<0.0001
λ_{21}	−1.5636	0.4159	459	−3.76	0.0002

Standard deviation estimates:
Random effects: $\hat{\sigma}_{MC0} = 0.0246, \hat{\sigma}_{\Delta MC1} = 0.0357, \ \hat{\sigma}_{\alpha 1} = 0.1633, \ \hat{\sigma}_{\Delta MC2} = 0.0360, \hat{\sigma}_{\alpha 2} = 0.2618.$
Residual: $\hat{\sigma}_{\varepsilon} = 0.0067.$

where x_1 is the tylosis fraction and x_2 is the specific gravity. Similarly, we can do the same for specific gravities across a range of tylosis fraction. For the term $\beta_{01} + \beta_{11} + \beta_{0,1*2}x_2$, conditional 95% confidence intervals can be estimated and tested with contrasts.

Figure A6(a) illustrates the tylosis coefficient estimate at each given specific gravity, plus their approximate 95% associated confidence interval at each specific gravity value. Note: these intervals are not adjusted for simultaneous inference at multiple specific gravity values, but they can help us determine approximately where the coefficient may be different from zero. For example, at low specific gravities, it appears the tylosis coefficient estimate is positive, implying that final MC increases with tylosis fraction. At higher specific gravities, the opposite appears to happen, with the tylosis coefficient being negative and implying the final MC will decrease with increased tylosis fraction. The relationship explains why at first it appeared that tyloses did not influence the final moisture contents as it appears to have opposing relationships centered around the average specific gravity. Similarly, the same can be performed to examine how specific gravity may affect the asymptotic MC at a given level of blockage by tyloses. Figure A6(b) shows the specific gravity coefficient estimate with a 95% conditional confidence interval at a given level of tylosis fraction. At higher tylosis levels, specific gravity has an increasingly negative relationship with final moisture contents; whereas at the lower tylosis levels, it does become positive, but not significantly different from zero. These relationships do appear to capture, for the most part, what was illustrated in the co-plots of Fig 7(a)-(c). Based on the contour plots (and the coefficient plots), it appears that the model predicts specific gravity and tyloses to interact to form a saddle point that shifts over time toward the average specific gravity and a lower level of tyloses. This indicates that some sort of trade-off is occurring in the uptake of water that likely balances inflow and diffusion.